Fuel and Equivalence Ratio Effects on Transfer Functions of Premixed Swirl Flames

Francesco Di Sabatino * and Thibault F. Guiberti †
King Abdullah University of Science and Technology, Clean Combustion Research Center, Thuwal 23955-6900, Saudi Arabia

Jonas P. Moeck ‡
Norwegian University of Science and Technology, Department of Energy and Process Engineering, 7491 Trondheim, Norway

William L. Roberts § and Deanna A. Lacoste ¶
King Abdullah University of Science and Technology, Clean Combustion Research Center, Thuwal 23955-6900, Saudi Arabia

This paper reports on the effects of fuel and equivalence ratio on the response of lean premixed swirl flames to acoustic perturbations of the flow, at atmospheric pressure. The response is analyzed using flame transfer functions, which relate the relative heat release rate fluctuations from the flame to the relative velocity fluctuations of the incoming flow. Two fuels, propane and methane, and five equivalence ratios are considered. The ten flames investigated are selected to exhibit the local maximum of the transfer function gain around the same frequency, 176 Hz. The results show that changing fuel and equivalence ratio influences both the gain and the phase of the transfer function. The changes observed at 176 Hz, where the dynamics of the flame is mainly controlled by the flame vortex roll-up mechanism, are discussed. Based on the analysis of the flow fields and the flame wrinkling, the laminar burning velocity and the flame temperature are identified as the main parameters controlling the gain. They have two competing effects: first, by enhancing the flame vortex roll-up and second, by affecting the strength of the vortex generated by the acoustic forcing due to changes in the height of the flame stabilization location.

Nomenclature

A = cross-section area of the vortex (m^2)

C = contour around the vortex (m)

*PhD Candidate, KAUST, CCRC.
†Research Scientist, KAUST, CCRC.
‡Associate Professor, NTNU, Energy and Process Engineering.
§Professor, KAUST, CCRC.
¶Assistant Professor, KAUST, CCRC.

d = stabilization distance of the flame from the nozzle tip (mm)

$\boldsymbol{dA}$ = element of the cross-section area A (m^2)

$\boldsymbol{ds}$ = element of the contour C (m)

f = frequency (Hz)

f_1 = frequency of the local minimum of the FTF Gain (Hz)

f_2 = frequency of the local maximum of the FTF Gain (Hz)

G = gain of the flame transfer function

L = characteristic flame length (m)

$\mathcal{L}$ = Markstein length (mm)

Le = Lewis number

P_{th} = thermal power of the flame (kW)

$\overline{\dot{Q}}$ = mean heat release rate (W)

$\dot{Q}'$ = heat release rate fluctuations (W)

R = radius of curvature of the flame front (mm)

Re = bulk Reynolds number

S = strain rate tensor (1/s)

S_L = laminar burning velocity (m/s)

St = Strouhal number

T_{ad} = adiabatic flame temperature (K)

T_u = temperature of the unburnt gases (K)

$\mathbf{u}$ = velocity vector (m/s)

$\overline{u}$ = mean flow velocity (m/s)

u' = velocity fluctuations (m/s)

$\bar{u}_{bulk}$ = average bulk velocity (m/s)

ϕ = equivalence ratio

Φ = phase of the flame transfer function (rad)

Γ = circulation of the acoustically generated vortex (m^2/s)

Γ_{max} = maximum circulation of the acoustically generated vortex (m^2/s)

$\frac{\partial u}{\partial t}$ = time derivative of the velocity at the hot wire location (m/s^2)

κ = curvature of the flame front (m^{-1})

$\boldsymbol{\omega}$ = vorticity vector (1/s)

Ω = vorticity tensor (1/s)

θ = phase within a forcing cycle (°)

I. Introduction

In recent years, there has been an increasing interest for lean premixed combustion in gas turbines, in order to reduce pollutant emissions and increase efficiency [1]. However, this technology is susceptible to thermoacoustic instabilities that can be very detrimental to the life cycle of the gas turbine and its efficiency. These instabilities result from the constructive interference between the acoustic modes of the combustor and the unsteady heat release rate from the flame [2–7]. Therefore, understanding the response of flames to acoustic perturbations is a prerequisite for solving problems of thermoacoustic coupling in gas turbines and aero-engines.

Flame transfer functions (FTFs) are the main concept in describing and analyzing the response of flames to small perturbation amplitudes [8–11]. An FTF compares the relative heat release rate fluctuations of a flame, $\dot{Q}'/\overline{\dot{Q}}$, to the relative velocity perturbations of the incoming flow, $u'/\overline{u}$. The FTF can be expressed as a function of the forcing frequency, f [10]:

$$F(f) = \frac{\dot{Q}'/\overline{\dot{Q}}}{u'/\overline{u}} = G(f)\, e^{i\Phi(f)}. \tag{1}$$

It is usually described with a gain, $G(f)$, and phase, $\Phi(f)$, which are both a function of the forcing frequency.

The parameters controlling the FTF are numerous, and expensive experiments, or simulations, are necessary to obtain an FTF at a given operating condition. In other words, it is not realistic to conduct experiments or simulations for every operating condition of a gas turbine. Therefore, it is necessary to develop simple relations or models to predict the FTF from parameters that can be easily measured or calculated. This has been the topic of several studies [12–20], where parameters such as flame length and flame base angle are used to characterize the flame's response to acoustic forcing.

For premixed swirl flames at atmospheric pressure, FTFs are well understood on a qualitative level. The constructive/destructive interactions between the roll-up of the flame tip around a vortex shed at the injector lip during the forcing period, called the flame vortex roll-up (FVR) [6, 13, 15, 16, 19, 21–23], and the fluctuations of the swirl number [15, 18], control the flame response. Typically, the FTF gain features two local maxima and a local minimum. The main mechanism driving the flame response is the FVR, but the local minimum is issued from swirl number fluctuations affecting the lower region of the flame. The frequency f_1 for which swirl number fluctuations are the largest, *i.e.* for which the FTF gain is locally minimal, is a function of the mean flow velocity, $\overline{u}$, and the distance between the swirler and the injector lips. The frequency f_2 for which the FVR is the most intense, *i.e.*, for which the FTF gain is locally maximal, is defined by a Strouhal number $\mathrm{St}_2 = f_2 L/\overline{u} \simeq 0.5$ [15, 17, 24], where L is a characteristic flame length. The phase of the FTF is generally proportional to the forcing frequency with a constant slope [25, 26].

If the forcing amplitude is relatively small, the FTFs are insensitive to the forcing amplitude (linear response). For

amplitudes larger than a threshold value (which depends on the operating conditions), saturation of the FTF gain occurs, and this is due to a combination of two mechanisms: (1) saturation of the shear layer instability, and (2) annihilation of the flame sheets [14, 19].

Several studies focused on the interactions between a swirl-stabilized flame and the acoustically generated vortex (AGV), that drive the FVR and control the maxima of the gain [18, 19, 27, 28]. Palies *et al*. [27] showed that the fluctuations of the flame base angle may interact with the development of the AGV. In this case, the strength of the FVR is affected by this interaction. Similar to [27], Bunce *et al*. [18] suggested that when the position of the flame base fluctuates close to the shear layer at the nozzle tip, the strength of the AGV is reduced due to thermal effects. In both studies, even if different values of pressure, inlet temperature, and equivalence ratio are considered, their respective effects on the FVR are not analyzed. Oberleithner *et al*. [19] experimentally investigated the response of a swirl flame to acoustic forcing for different forcing amplitudes through the stability analysis of the shear layer from which the AGV is shed. They showed that the receptivity of the shear layer controls the size of the AGV and consequently the gain magnitude. However, the effects of fuel and equivalence ratio on the FVR are not analyzed in any of these studies.

Effects of fuel and equivalence ratio on the FTF of premixed swirl flames have also been the topic of a few studies [16, 18, 29, 30] but a satisfactory explanation of the observed trends is not always provided. The main challenge is that changing fuel or equivalence ratio affects important flame properties such as its length and, as a consequence, both the magnitude of the gain and frequencies f_1 and f_2 usually change [15, 17]. It is then difficult to identify what the relevant fuel parameters are that should be considered for predicting the propensity of a fuel to promote thermoacoustic coupling. For premixed laminar flames, Gaudron *et al.* [20] have shown that, depending on the burner dimensions, the Lewis number, the laminar burning velocity, the flame thickness, and the flame temperature can play a role in the response of laminar flames to acoustic forcing. In a similar manner, it would be interesting to determine the relative impact of such properties on the FTF of turbulent premixed swirl flames.

In this context, the main objectives of the present study are: a) to analyze the effects of fuel and equivalence ratio on the FTF of premixed swirl flames, and b) to identify the key parameters responsible for the fuel and equivalence ratio effects on the FVR. Understanding these effects could be of practical interest for engine designers. Indeed, changes in the fuel formulation or in equivalence ratio may have a dramatic impact on the flame stability, and therefore on the behavior and performances of the gas turbine or aero-engine. Developing simple models for the effects of fuel and equivalence ratio on the flame response to acoustic perturbation could be a valuable tool for the aerospace propulsion community.

II. Experimental Setup and Procedure

A. Premixed Swirl-stabilized Burner and Experimental Conditions

The schematic of the burner used in this study is presented in Fig. 1. A detailed description can be found in Lacoste *et al*. [31] and Di Sabatino *et al*. [32]. The gaseous fuel and air are premixed 2 meters before being injected into a plenum of 120 mm length. This ensures that no equivalence ratio fluctuations are present during the acoustic forcing of the flame. The flow of reactants is regulated by thermal mass flow controllers (Brooks SLA 58 Series). Reactants then flow through a honeycomb section and a perforated plate before entering a radial swirler. The swirler features a measured swirl number of 0.39 [33], following the definition of [34]. The injection tube has a diameter of 18 mm and includes a central rod with a diameter of 2.5 mm. A small diameter for the central rod is chosen in order to be close to a purely aerodynamically stabilized condition. This choice, associated with a relatively small swirl number, simplifies the problem, as the inner recirculation zone (downstream of the rod) can be ruled out of any stabilization mechanism. The flame is stabilized downstream of the injection tube and a quartz tube of 100 mm length and 70 mm inner diameter confines it.

The acoustic section of the burner is composed of a 900 W loudspeaker (Beyma 10LW30/N) mounted in a 15.4 L plastic enclosure and powered by a high-fidelity amplifier (QSC GX5). A signal generator (NF WF1973) connected to the amplifier allows the control of the frequency and the amplitude of the acoustic forcing of the flow of reactants.

Table 1 Summary of the experimental conditions.

Fuel	ϕ	P_{th} (kW)	$\bar{u}_{bulk}$ (m/s)	Re	S_L (m/s)	T_{ad} (K)
CH_4	0.65	3.8	6.4	7,400	0.15	1754
	0.67	3.9	6.4	7,400	0.16	1788
	0.70	4.0	6.4	7,400	0.19	1839
	0.73	4.0	6.2	7,100	0.22	1888
	0.76	4.2	6.2	7,100	0.25	1935
C_3H_8	0.69	4.4	6.5	8,000	0.20	1863
	0.70	4.4	6.5	8,000	0.22	1880
	0.74	4.7	6.5	8,000	0.24	1947
	0.79	4.7	6.3	7,600	0.30	2027
	0.83	5.0	6.3	7,600	0.32	2087

The different fuels and equivalence ratios, and their corresponding thermal power (P_{th}), bulk velocity ($\bar{u}_{bulk}$), bulk Reynolds number (Re), laminar burning velocity (S_L), and adiabatic flame temperature (T_{ad}), examined in this study are summarized in Table 1. The values of S_L are determined by averaging the values from [35–40] with those calculated with Cantera [41] for a freely propagating flame with an initial temperature of 300 K using the USC-II mechanism [42] and a mixture-averaged mass diffusion model. These ten flames are selected to exhibit the local extrema

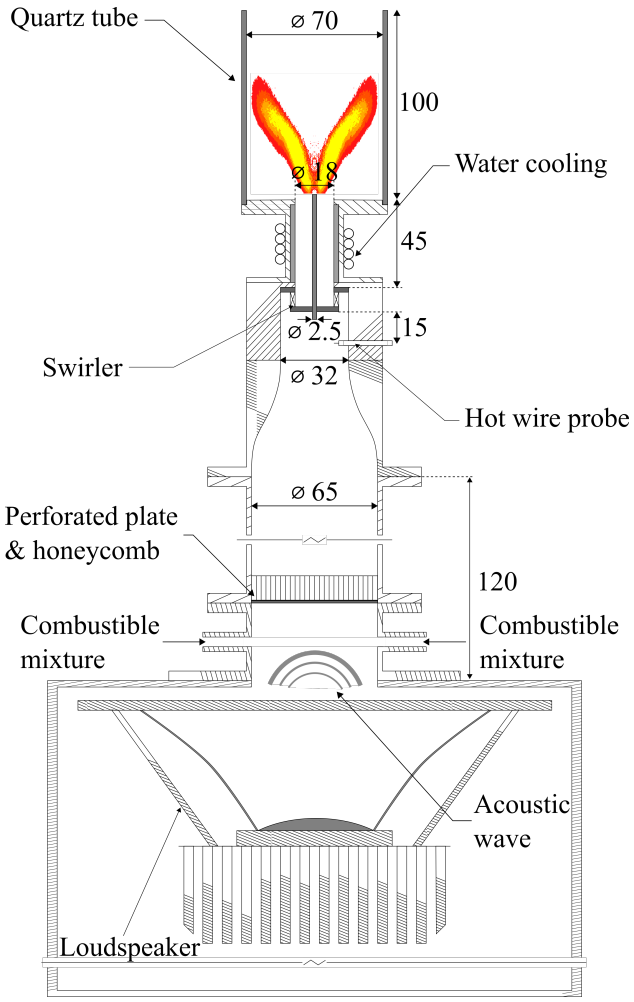

Fig. 1 Schematic of the burner. All dimensions are given in millimeters.

of the gain of the flame transfer function around the same frequencies. This is done to yield meaningful comparisons between all the cases. Indeed, if the extrema were not obtained for fixed frequencies, the driving mechanisms of the flame responses to acoustic modulation of the flow would have been combined in a different way for each condition. Consequently, a quantitative analysis of the effect of fuel and equivalence ratio would have been extremely challenging. Direct time-averaged images recorded with a DSLR camera for all the flames investigated are shown in Fig. 2.

B. Diagnostics

The FTF can be evaluated from the velocity oscillations and the global heat release rate fluctuations of the flame subjected to acoustic forcing. A hot wire (Dantec miniCTA) is used to measure the velocity oscillations 1 cm upstream of the swirler, corresponding to about 7 cm upstream of the outlet of the injection tube. Altough the velocity fluctuations should ideally be measured at the flame location, it has been shown in a previous study using a similar setup [15] that measuring them upstream of the swirler does not introduce significant modifications to the FTF for forcing frequencies

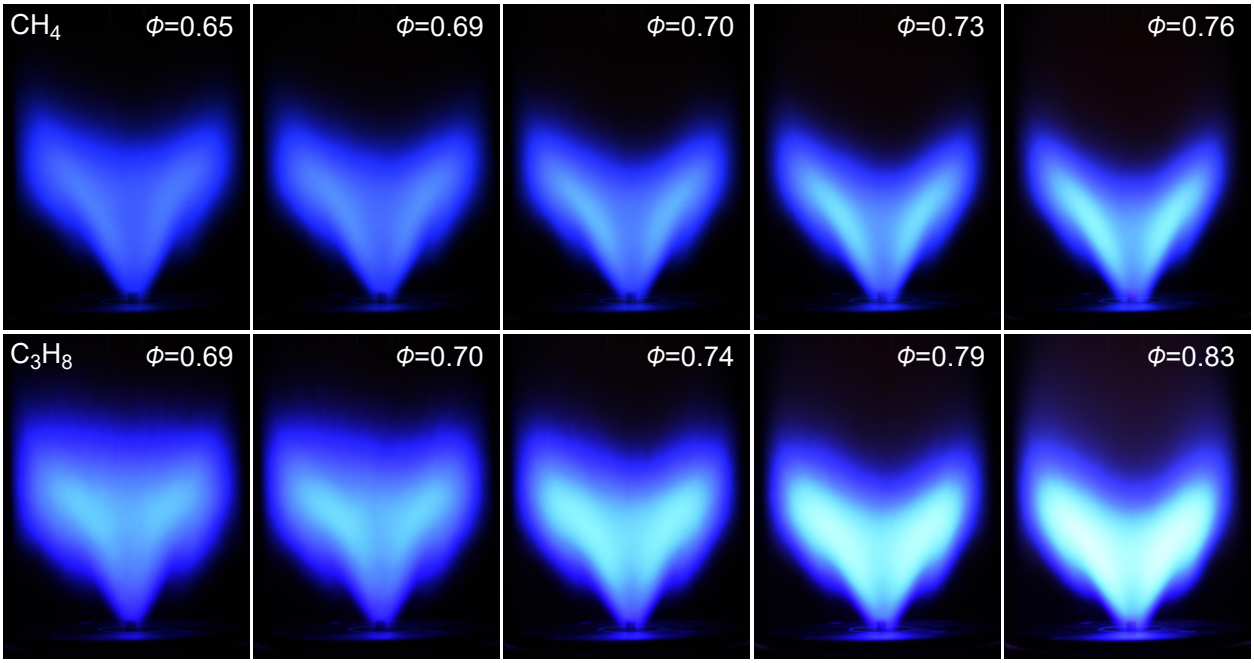

Fig. 2 Photographs of the flames considered in this study. The exposure time is 1.6 s for all these images.

smaller than 1 kHz. A difference in the magnitude of the gain of less than 10% and a difference in the slope of the phase of less than 5% are observed. These differences would apply equally to all the experimental conditions analyzed so the general trend of the results would be maintained.

Since only perfectly premixed flames are considered in this study, the heat release rate fluctuations are determined from the global OH^* chemiluminescence of the flame [43]. A photomultiplier tube (Hamamatsu H10721), equipped with a 10 nm bandpass filter centered at 310 nm (ZBPA310 ASAHI Spectra Co.) is used to measure the fluctuations of OH^* chemiluminescence. It has been shown in previous studies [15, 17, 44] that this technique can be used for non-adiabatic combustors and the errors introduced in doing so are not of first order. The hot wire signal, the photomultiplier tube (PMT) signal, and the forcing signal are recorded using an oscilloscope (Agilent Technologies Infiniium 2.5 GHz).

The flame dynamics during acoustic forcing is captured by collecting the OH^* chemiluminescence with an intensified CCD camera (Princeton Instruments PI-MAX) equipped with a UV lens (105 mm Coastal Optics) and a 10 nm bandpass filter centered at 310 nm (ZBPA310 ASAHI Spectra Co.). The exposure time is kept equal to 200 μs in all cases. The camera is synchronized with the signal generator controlling the acoustic forcing, allowing the collection of images during different specified phases of the forcing period.

The velocity fields are measured by particle image velocimetry (PIV). The PIV system comprises a 10 Hz dual pulse Nd:YAG laser (Litron Nano L200-15 PIV), that generates a laser beam of 26 mJ per pulse at 532 nm, and a 1200×1600 pixels dual frame CCD camera (LaVision Imager Pro X). The camera is equipped with a lens (60 mm AF Micro Nikkor) and a 10 nm bandpass filter centered a 532 nm (LaVision VZ17-0117). The laser beam is converted into a laser sheet

of about 1 mm thickness and 60 mm height trough a combination of spherical and cylindrical lenses. The laser sheet is focused along the central axis of the burner allowing the measurement of the axial and radial components of the velocity field. The flow of reactants is seeded with titanium dioxide (TiO_2) particles featuring an average diameter of around 3 μm. The images are processed with a multi-pass technique (LaVision DaVis 8.4.0) with a 16×16 pixels final interrogation area and 50% overlap, yielding a vector spacing of 0.4 mm. The PIV system is synchronized with the signal generator controlling acoustic forcing to measure phase-locked velocity fields during the forcing period.

Finally, OH planar laser induced fluorescence (OH-PLIF) imaging of the flames has been conducted to infer the flame front position and curvature as a function of fuel, equivalence ratio, and phase of the modulation period. The 10-Hz OH-PLIF system used is fairly standard and the interested reader is referred to [45] for more details. The laser sheet for the OH-PLIF overlaps that of the PIV but has a thickness of around 200 μm.

C. Experimental Procedure

For each experimental condition, the flame is first ignited and run for at least 15 minutes to ensure that thermal steady state is reached. The acoustic forcing of the flow of reactants is then started, and the amplitude of the forcing signal is adjusted to obtain a velocity fluctuation amplitude equal to 10% of the mean flow velocity. A 10% amplitude has been chosen to ensure the linear response of the flames to the acoustic forcing while overcoming the natural level of turbulent fluctuations, which is about 5%. The frequency of the forcing signal is increased from 32 Hz to 400 Hz by steps of 16 Hz. The forcing signal, the velocity signal measured with the hot wire, and the OH^*chemiluminescence signal collected with the PMT are simultaneously recorded for 10 s with a sampling frequency of 20 kHz and are used to compute the FTF.

The flame dynamics and the velocity fields are collected and analyzed at the forcing frequency of 176 Hz. This frequency is chosen because it corresponds to the local maximum of the gain of the FTF. This is also where the influence of the fuel and ϕ will be investigated in detail. To collect phase-locked images of OH^* chemiluminescence, OH-PLIF, and velocity fields, the forcing period is divided into 10 phases, θ, with an interval of 36^o each. The phase $\theta = 0^o$ is selected when $u' = 0$ and $\frac{\partial u}{\partial t} > 0$ at the position of the hot wire.

To investigate the flame dynamics, 1000 images of OH^* chemiluminescence are collected for each of the ten phases of the forcing period and are then averaged to ensure statistical convergence. After checking that the flame is axisymmetric on average, a radius-weighted Abel-deconvolution is applied to evaluate the distribution of the OH^* chemiluminescence intensity in the central longitudinal plane. A similar procedure is followed with the measured velocity fields. To ensure statistical convergence, 800 instantaneous velocity fields are averaged for each of the ten phases of the forcing period. The phase-averaged velocity fields are smoothed using a 5×5 pixel Gaussian filter. The coherent flow structures, *i.e.*, the outer recirculation zone (ORZ) and the vortex generated by acoustic forcing (AGV), are identified in the phase-averaged velocity fields using the Q-criterion [19, 46]. The quantity Q is defined as $Q = 0.5(||\Omega||^2 - ||S||^2)$, where Ω and S are vorticity tensor and strain rate tensor, respectively. The Q fields of each experimental condition are then normalized with

respect to the overall maximum value, which is obtained for the unforced propane flame with $\phi = 0.70$. Furthermore, a total of 750 OH-PLIF images are recorded for each condition examined. Raw images are first corrected for background noise, and a binarized flame front is then extracted using a Canny edge-detection algorithm. The signed curvature is finally computed at each flame front position and for each available OH-PLIF image. Due to the limited optical resolution of the OH-PLIF arrangement (roughly 0.4 mm), the maximum curvature measurable is estimated to be $|\kappa| = 2500\ \mathrm{m}^{-1}$.

III. Results

A. Flame Transfer Functions

The transfer functions of the flames considered in this study (see Table 1) are presented in Fig. 3. Both gain

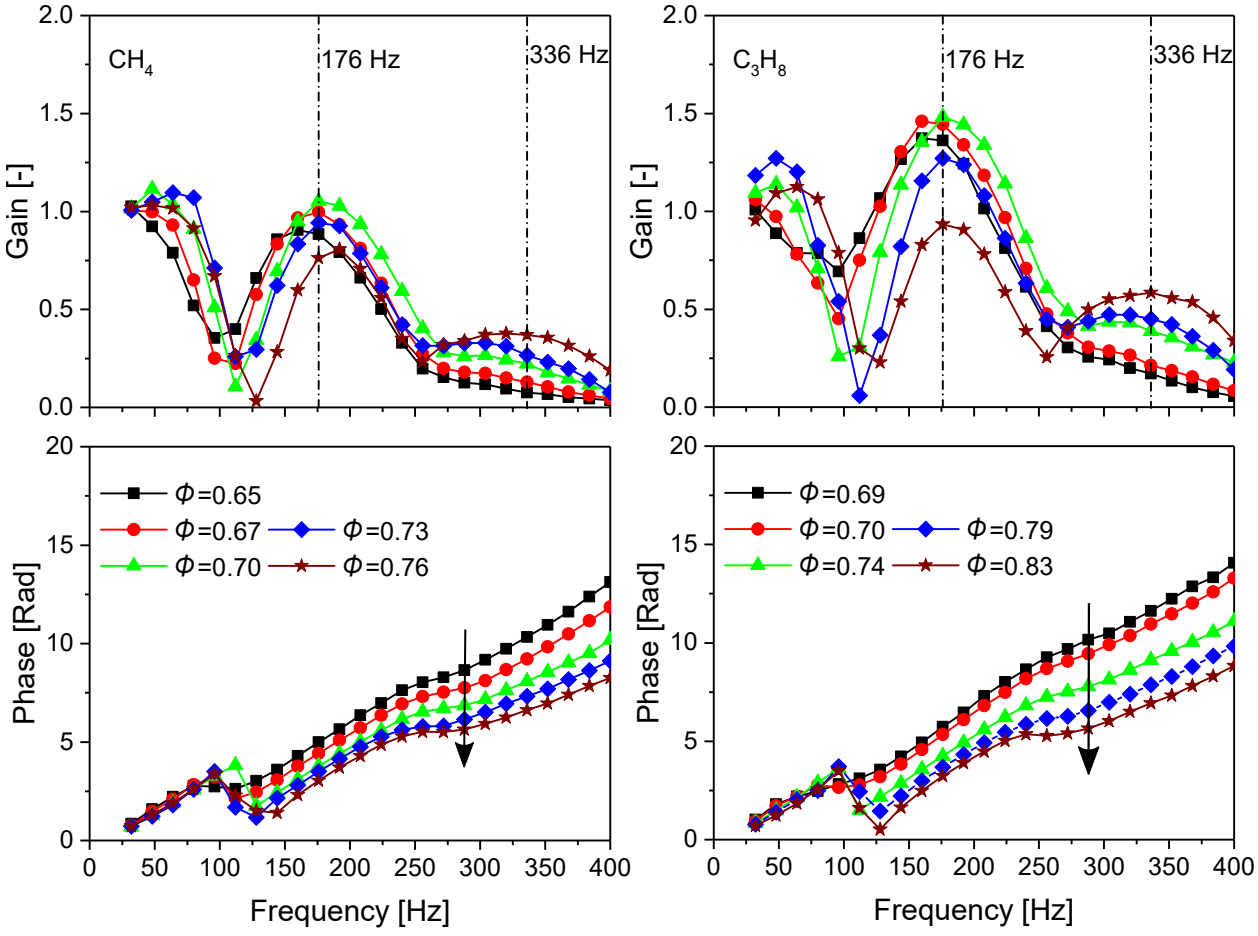

Fig. 3 Flame transfer functions of methane (left) and propane (right) premixed swirl flames at 10% of forcing amplitude. Arrows indicate trends with increasing equivalence ratio.

and phase show the trend that is typical for swirl flames. At low frequency, the gain approaches one and the phase approaches zero [47]. Focusing on the gain, a local minimum is found at 112 Hz followed by a local maximum at

176 Hz [15, 17, 32, 48, 49]. The competition between the fluctuations of the bottom region of the flame, generated by the oscillations of the flame base angle driven by the fluctuations of the swirl number [15, 18], and the oscillations of the top region due to flame vortex roll-up [6, 13, 15, 19, 21–23], generates this distinctive trend of the gain. The phase shows a linear trend for frequencies ranging from 32 Hz to 112 Hz. Around 112 Hz, the phase decreases suddenly but then resumes its linear increase for frequencies above 128 Hz. This sudden decrease of the phase is observed at around the same frequency of the first local minimum of the gain [11]. Since the flame transfer function is a smooth complex-valued function, a zero in the gain is thus naturally accompanied by a phase jump.

Having presented the general trend of the gain and phase of the FTF, the effect of equivalence ratio can now be detailed. As shown in Fig. 4 (right), for all the equivalence ratios investigated, the extrema of the gain do not show any significant shift in frequency. Note that the bulk velocity has been slightly adjusted for the highest values of ϕ for both fuels to maintain similar values of frequency for the extrema of the gain. At its first maximum (64 Hz), the gain magnitude first increases with the equivalence ratio up to $\phi = 0.73$ for methane, and $\phi = 0.79$ for propane, but then decreases. Similar behavior can be observed at the frequency of the second gain maximum (176 Hz), but with more pronounced effects. Finally, around 336 Hz, the gain monotonically increases with the equivalence ratio. No clear trend can be revealed at the local minimum of gain near 112 Hz. These trends are highlighted in Fig. 4 (left). Similar behavior is observed for both fuels although propane flames show globally higher gain responses, especially for frequencies around 176 Hz. For both fuels, at frequencies lower than 112 Hz, the phase is not affected by the change in equivalence ratio, while for higher frequencies it decreases with equivalence ratio, as highlighted by the black arrows in Fig. 3. In the interest of conciseness, only the effects of fuel and equivalence ratio at 176 Hz, where the gain magnitude is large, are analyzed and discussed. The analysis of the trends obtained at 336 Hz can be found in [50].

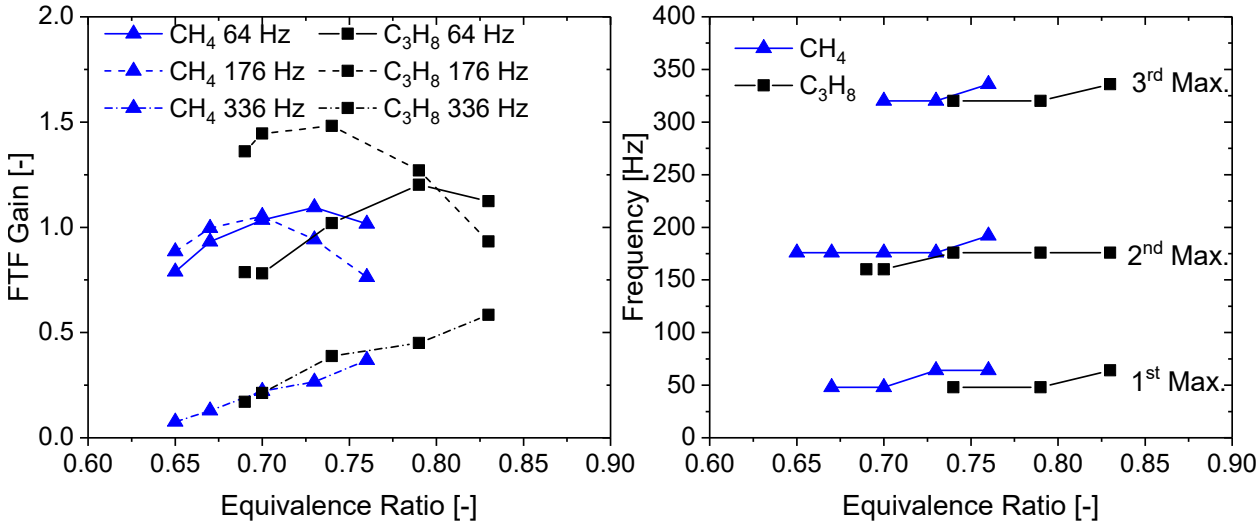

Fig. 4 FTF gain (left) and frequency (right) of the local maxima as a function of equivalence ratio.

B. Flame Dynamics

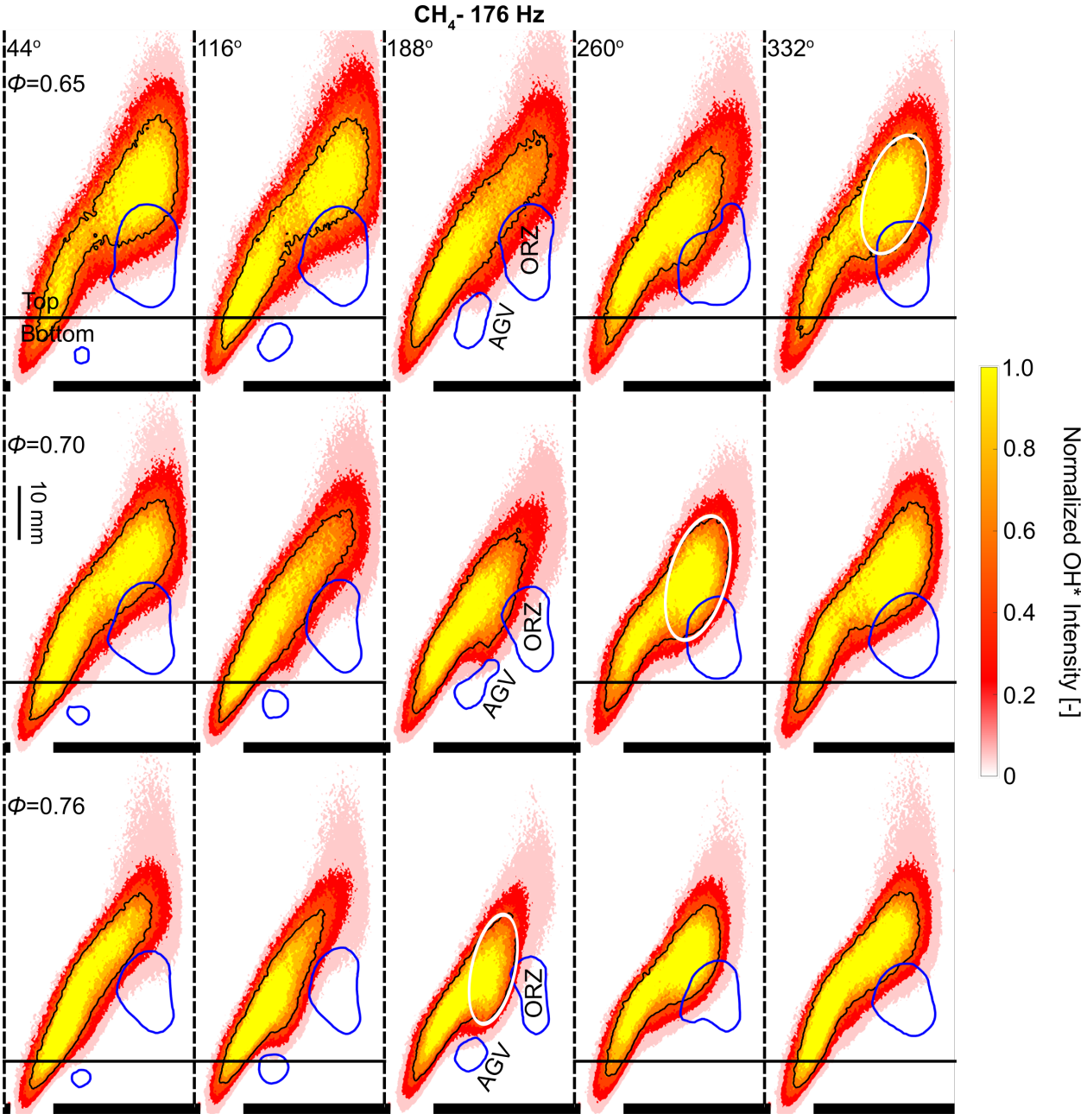

Fig. 5 Phase-locked 0.5 iso-contours of normalized Q-criterion superimposed to the normalized phase-averaged radius-weighted Abel-deconvoluted OH* chemiluminescence intensity of methane flames at 10% forcing amplitude.

The phase-locked radius-weighted Abel-deconvoluted images of OH* chemiluminescence are shown in Figs. 5 (methane) and 6 (propane). For clarity, only one phase each 72° is presented. The phases that are not shown in these figures do not provide any additional information to the motion of the AGV and to the analysis of the results. These images are normalized with respect to the global maximum value of OH* chemiluminescence intensity at the same

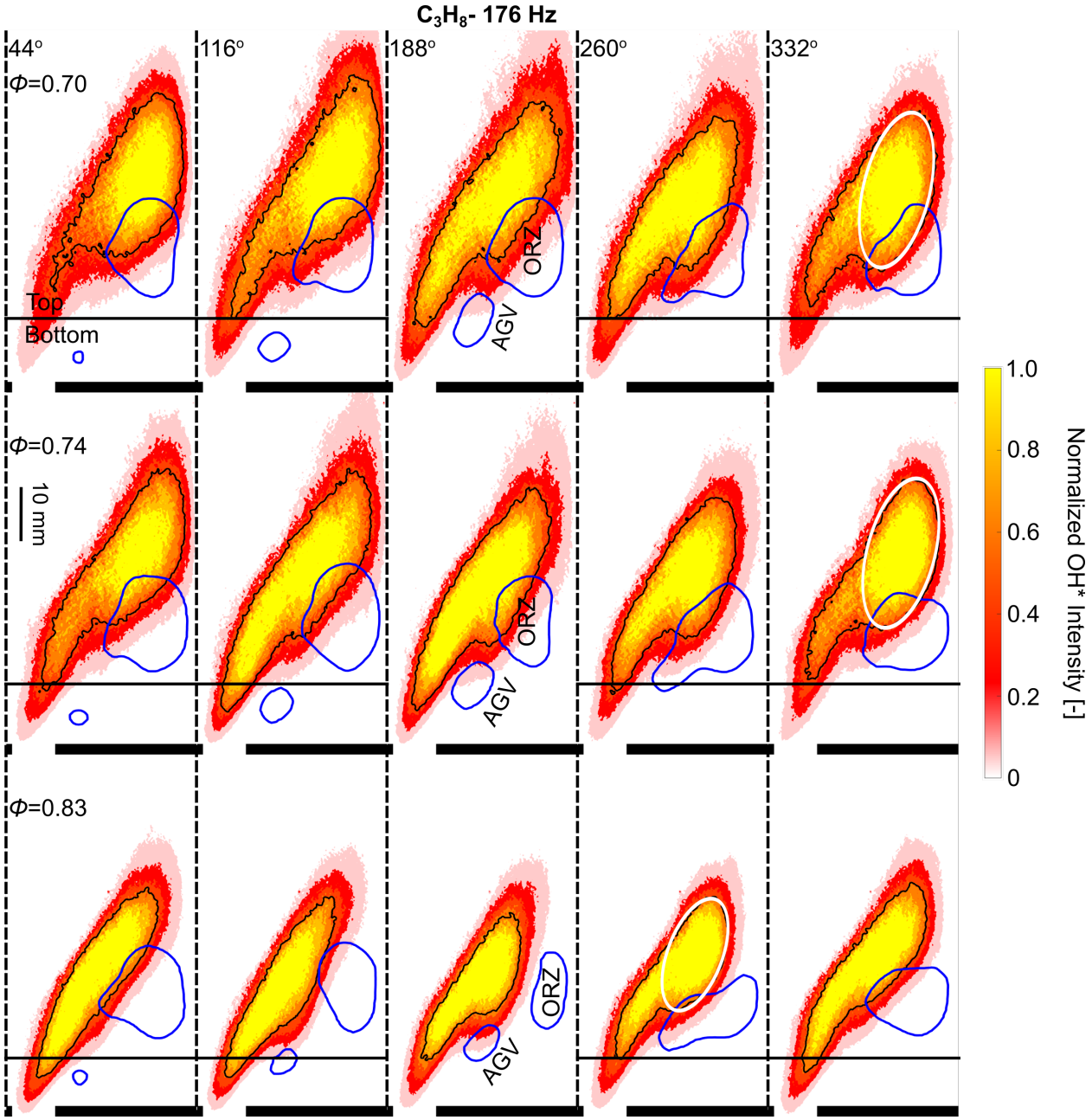

Fig. 6 Phase-locked 0.5 iso-contours of normalized Q-criterion superimposed to the normalized phase-averaged radius-weighted Abel-deconvoluted OH* chemiluminescence intensity of propane flames at 10% forcing amplitude.

equivalence ratio and for the same fuel. First, the phase-locked images are normalized, and then the radius-weighted Abel-deconvolution is applied. An iso-contour of 0.4 is highlighted in black to assist visualization of the flame motion. The iso-contour is calculated to delimit the surface area of the flame that accounts for 60% of the total intensity of the OH* chemiluminescence/heat release of the flame. It is used to highlight the flame boundaries in order to help in visualizing the flame dynamics and the flame vortex roll-up mechanism. As shown in a previous study [32], choosing a

different value for the iso-contour has no influence on the analysis and conclusions. The acoustically generated vortex (AGV) and the outer recirculation zone (ORZ) are also highlighted in these figures. The way they are determined is detailed in Sec. III.C.

As presented in the introduction, the FVR is an important mechanism that controls the flame response to the acoustic excitation at 176 Hz. In order to characterize the FVR for all the conditions investigated, an ellipse is fitted in the 0.4 iso-contour near the flame tip. The choice of an ellipse is dictated by the fact that it is the simplest geometrical shape that fits the best in the flame shape. Only the phase during the forcing period for which the perimeter of the ellipse is the largest is considered. For example, it is $\theta = 332^\circ$ for methane flames at $\phi = 0.65$ and $\theta = 260^\circ$ for propane flames at $\phi = 0.83$. Figures 5 and 6 show that modifying the equivalence ratio or the fuel has a large influence on the perimeter of these ellipses. Trends are examined in more detail in Sec. IV.

Each image has been divided into two regions by a solid black line: a top region above the line, that is positioned to include all the contributions of the flame vortex roll-up to the flame motion, and a bottom region below this line. This line can be slightly moved, up or down, without substantially changing the normalized integrated OH^* chemiluminescence intensity signals. The OH^* chemiluminescence intensity can be integrated over each of the top and bottom regions, and over the entire flame, for each forcing phase, fuel, and equivalence ratio in order to analyze flame dynamics in more detail. Results are shown in Fig. 7. Note that the results presented in this figure are obtained from the images without Abel deconvolution. These integrated OH^* chemiluminescence intensities are normalized by the value obtained by averaging over the same region and over the whole forcing period. This normalization procedure is used only to ease the comparison of amplitude of fluctuations and phase differences by having the mean value equal to one. The relative amplitude and phase are not modified by the normalization procedure. The error bars represent the range of amplitudes that the signals can exhibit, while slightly modifying the position of the solid black line.

For both fuels, the amplitude of the temporal fluctuations of the OH^* chemiluminescence intensity of the top region (blue squares) is two to six times larger than that of the bottom region (red circles), depending on fuel and equivalence ratio. This suggests that the dynamics of the top region is predominant. However, for the largest equivalence ratio (lowest row), and regardless of fuel, the relative contribution of the bottom region increases. An explanation for this behavior is provided in Sec. IV. On the other hand, the maximum difference between the amplitude of the temporal fluctuations of the OH^* chemiluminescence intensity of the top region (blue squares) and those of the entire flame (black triangles) ranges from 0.1 % to 5 %. This very small difference underlines that the dynamics of the bottom region is negligible compared to the one of the top region, even for cases where their fluctuations are out-of-phase (largest equivalence ratio).

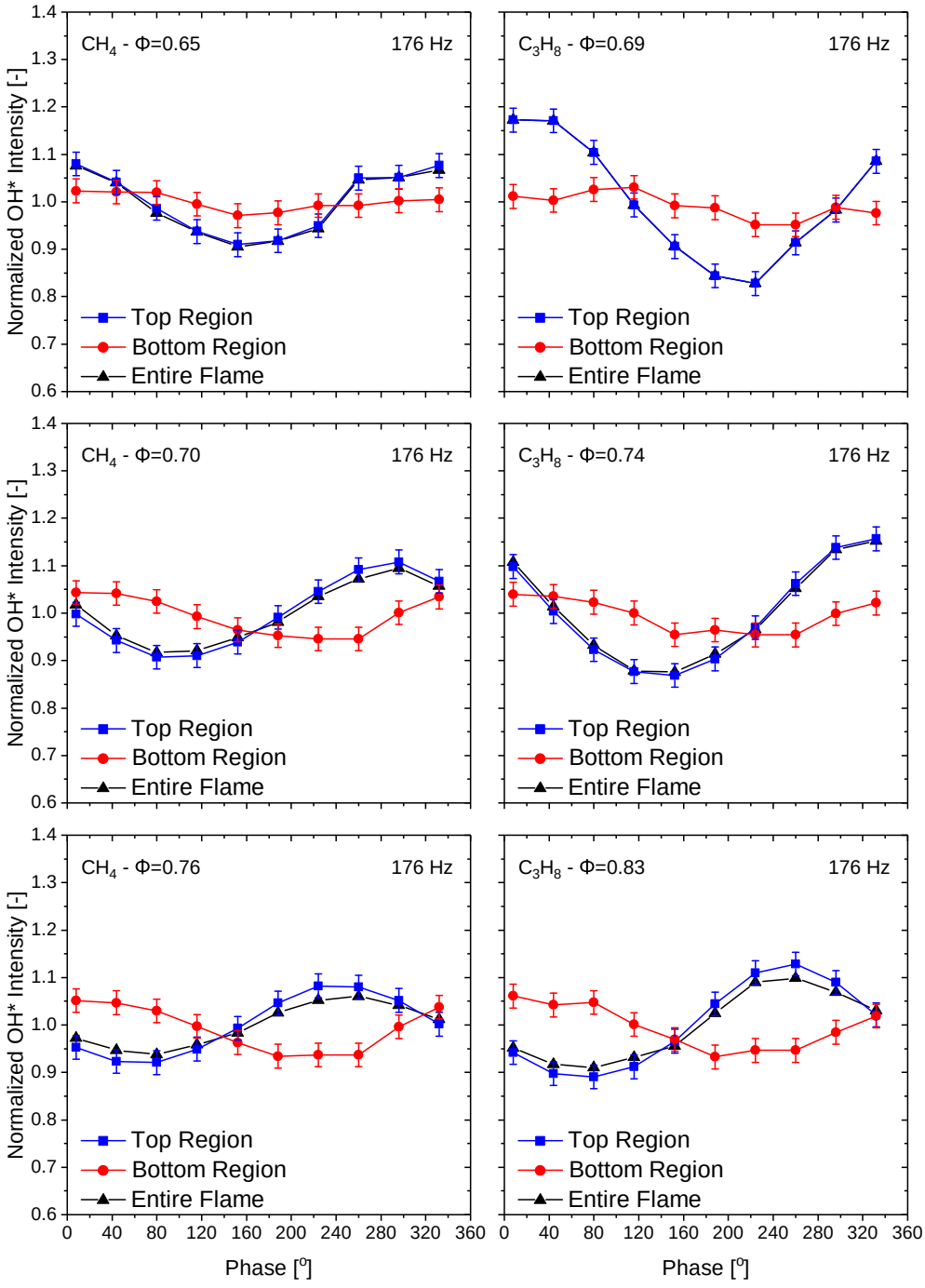

Fig. 7 Temporal fluctuation of the normalized OH* chemiluminescence integrated over the top (blue) and bottom (red) regions, and over the entire flame (black) for methane (left) and propane (right) flames.

C. Velocity fields

Examples of velocity fields measured without acoustic forcing are presented in Fig. 8 (left), for cold flows, and in Fig. 8 (right), for reactive cases. Typical features of cold and reactive swirl flows are observed, including: an inner recirculation zone (IRZ) enclosed by an annular jet (AJ) surrounded by an outer recirculation zone (ORZ). The ORZ is

highlighted by a 0.5 iso-contour of the normalized Q-criterion. Figure 8 (left) shows that changing the equivalence ratio, fuel, and/or bulk velocity (see Table. 1) has no noticeable influence on the cold flow fields. On the other hand (see Fig. 8 (right)), the presence of the flame substantially modifies the flow field by yielding higher velocities in the AJ, as well as modifying the IRZ and ORZ. In the presence of a flame, when ϕ is increased, the position of the ORZ shifts upstream while its size reduces. A similar trend is observed for both fuels. Comparing Figs. 8 (left) and 8 (right), it is obvious that the presence of the flame plays a major role in defining the velocity field and outweighs the small differences in bulk velocity between the different cases (see Table. 1).

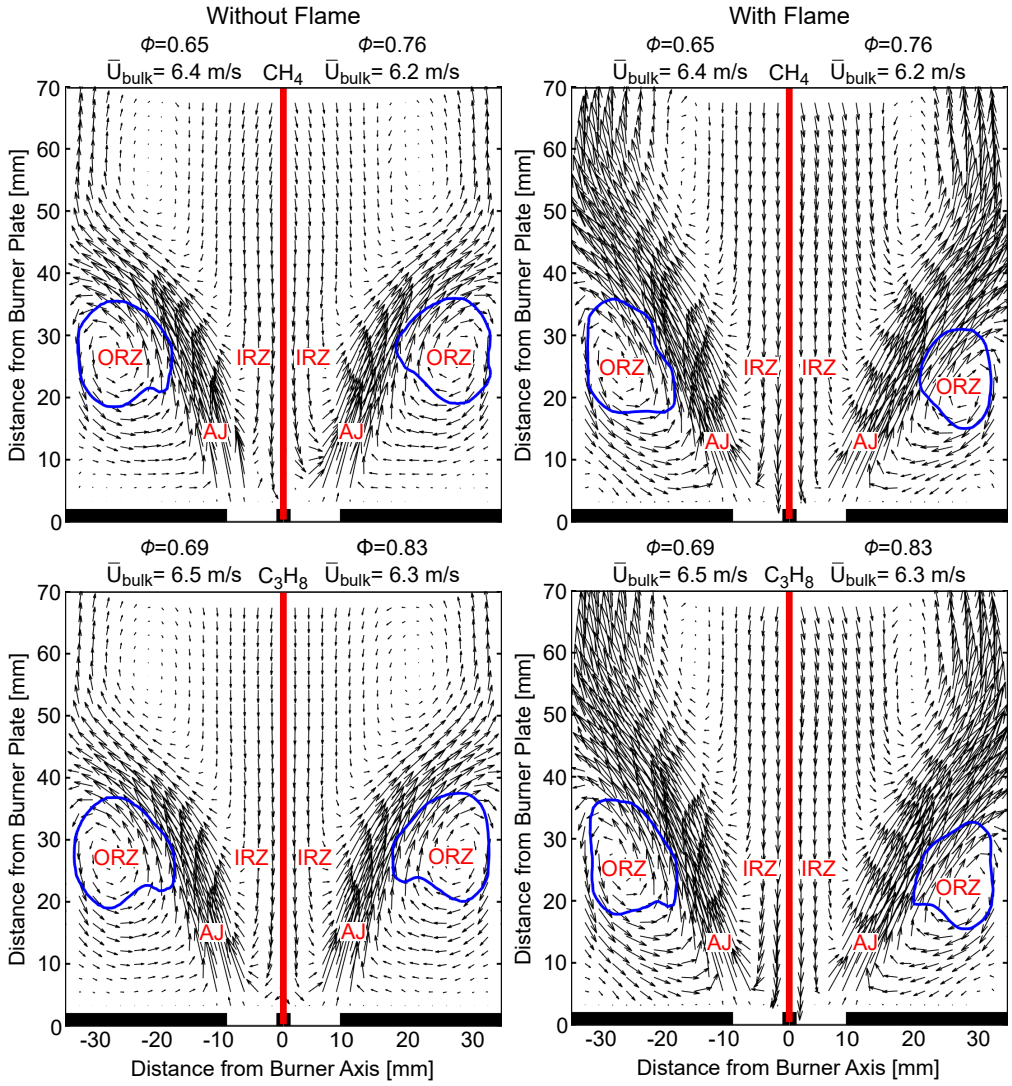

Fig. 8 Unforced mean velocity fields for methane (top) and propane (bottom) measured without (left) and with (right) flame.

To analyze the interactions between the flame, the AGV, and the ORZ, the phase-locked 0.5 iso-contours of the normalized Q-criterion are superimposed to the phase-locked normalized OH^* chemiluminescence intensity in Figs. 5 (methane) and 6 (propane). These figures highlight the evolution of the vortex generated by acoustic forcing. The vortex

is shed from the outer shear layer at the nozzle tip (around $\theta = 44°$). It then travels downstream, interacts with the flame and finally merges with the ORZ ($\theta = 260°$). Unfortunately, the Q-criterion is not able to track the AGV inside the ORZ. The size of the AGV increases with time during the forcing cycle and it reaches its maximum measurable value at $\theta = 188°$. Regardless of fuel, the maximum size of the AGV seems to decrease as the equivalence ratio is increased. The evolution of the AGV is analyzed in Sec. IV.

D. Flame Front Curvature

Lean premixed propane flames have a non-unity Lewis number (Le = 1.88). Consequently, it is important to assess whether or not differential-diffusion effects can play a role in the response of the flame to acoustic forcing. To investigate this potential effect, the probability density function (PDF), of flame front curvature (κ), should be determined. For this purpose, the forced-flame front curvature is measured by using OH-PLIF images. Figure 9(a) shows an example of instantaneous OH-PLIF image and flame front (color-coded to the signed curvature κ), for a propane flame with $\phi = 0.7$, at the phase $\theta = 332°$.

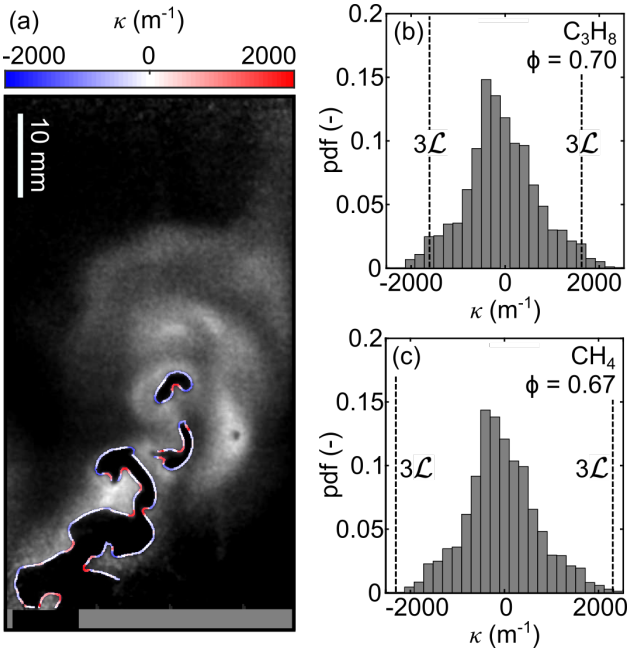

Fig. 9 (a) Snapshot of OH-PLIF and extracted flame front for propane with $\phi = 0.70$ and $\theta = 332°$. PDFs of curvature κ for propane (b) and methane (c).

The OH-PLIF snapshots are assembled in the 10 phase bins. The signed curvature of the flame front is measured for all snapshots with a certain phase and equivalence ratio, and the corresponding PDF is computed. This is shown, for example, in Figs. 9(a) and (b) for propane and $\phi = 0.70$ at $\theta = 332°$. Figure 9(c) shows the PDF of signed curvature for methane at $\phi = 0.67$ at $\theta = 332°$. The phase considered in Figs. 9(a)-(c) corresponds to the time of most intense flame vortex roll-up during the forcing period at 176 Hz. Both distributions of signed curvature κ are unimodal and

very similar. Values of κ are biased towards negative values. Therefore, concave flame sheets that are curved towards reactants are most probable, and this could be due to the flame topology. In addition, the curvature probability gradually decreases and reaches a zero value near $|\kappa| = 2000$ m^{-1}, which is below the detection limit of $|\kappa| = 2500$ m^{-1}, suggesting that the entire meaningful curvature dynamics is captured with the available OH-PLIF arrangement. Similar results are obtained for all the operating conditions considered in this study. These results are used in the next section to assess the impact of differential-diffusion on the dynamics of the lean propane flames that feature non-unity Lewis numbers.

IV. Discussion

The results presented in the previous sections are analyzed in more depth here. First, the dependency between the gain of the FTF at 176 Hz and the maximum size of the FVR is discussed. Then, parameters controlling the maximum size of the FVR are identified. Next, an explanation for the non-monotonic behavior of the FTF gain at 176 Hz when the equivalence ratio is increased is proposed. Finally, effects of fuel and equivalence ratio on the FTF phase are discussed.

A. Relation between FVR and FTF Gain

As shown in Fig. 7, the dynamics of the flame at 176 Hz is mainly controlled by the motion of its top region which is driven by FVR. However, the contribution of the bottom region to the flame dynamics increases with the equivalence ratio for both fuels. This trend could be attributed to the decrease in bulk velocity that is needed to maintain the local gain maximum at 176 Hz when the equivalence ratio is increased (see Tab. 1). Indeed, decreasing the bulk velocity usually results in the reduction of the frequency at which the temporal fluctuations of the swirl number are negligible [11, 15, 23, 51]. Since swirl number fluctuations are known to influence mainly the dynamics of the bottom region, it is possible that reducing the bulk velocity augments the dynamics of the bottom region due to the introduction of swirl number fluctuations at 176 Hz.

From the phase-locked OH* chemiluminescence images, the maximum perimeter of the flame vortex roll-up, referred to as $\mathrm{FVR_{max}}$ and defined by the white ellipses in Figs. 5 and 6, can be evaluated for all the conditions examined. This maximum perimeter is used as a measure of the maximum size of the flame vortex roll-up during the forcing cycle. The rolling up of the flame around the toroidal vortex shed at the nozzle tip due to the incoming acoustic wave modulates the flame surface area, and consequently the heat release from the flame. Therefore, the maximum size of the FVR during the forcing cycle, the $\mathrm{FVR_{max}}$, can be used as a metric of the impact of the FVR on the flame surface area, heat release, and flame dynamics. The magnitude of the FTF gain measured at 176 Hz is plotted as a function of $\mathrm{FVR_{max}}$ in Fig. 10 (top). Figure 10 shows that the magnitude of the FTF gain at 176 Hz is proportional to $\mathrm{FVR_{max}}$. This result is in agreement with that of [32] for the dynamics of similar flames at elevated pressure. The error bars in Fig. 10 represent the uncertainty in the fitting process of the ellipse into the 0.4 iso-contour of normalized OH* chemiluminescence intensity. Figure 10 (bottom) plots the magnitude of the FTF gain measured at 176 Hz as a function of $\mathrm{FVR_{max}}$ if only

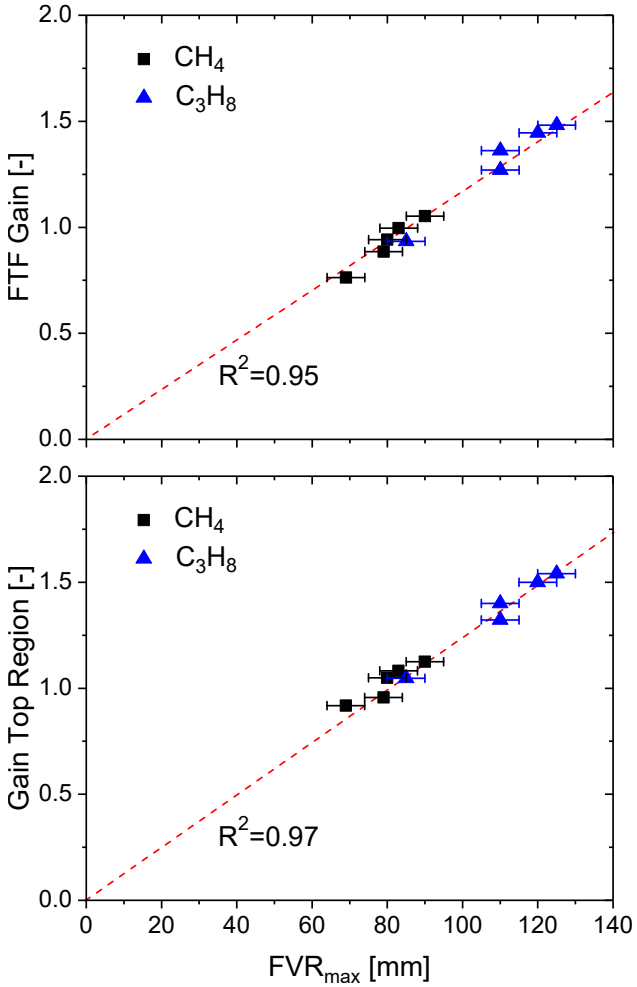

Fig. 10 Top: FTF gain at 176 Hz as a function of FVR_{max} for all the flames considered in this study. Bottom: FTF gain at 176 Hz as a function of FVR_{max} if only the contribution of the top region is accounted for.

the contribution of the top region to the OH^* signal is accounted for. This can be achieved by using the top region of the phase-locked OH^* chemiluminescence images (without Abel deconvolution), instead of the photomultiplier tube signal to compute the FTF gain. The magnitude of the FTF gain at 176 Hz remains proportional to FVR_{max}, which confirms that flame vortex roll-up in the top region of the flame controls the flame dynamics. Therefore, in order to quantify the effects of fuel and equivalence ratio on the FTF gain at 176 Hz, it is important to understand the effects of fuel and equivalence ratio on FVR.

B. Effects of Differential-diffusion

For a non-unity Lewis number mixture, such as the lean propane–air mixtures examined here, the burning velocity and the heat release rate can be affected by the local flame curvature, which may in turn affect flame dynamics and FTF gain. However, such differential-diffusion effects can only occur if the local flame radius of curvature is comparable to the Markstein length [52]. In their investigations of the dynamics of laminar premixed lean propane conical flames,

Gaudron *et. al.* [20] observed that differential-diffusion starts to play a role for a small circular injector with a diameter of 1.5 mm and that this was due to significant curvature near the conical flame tip. Careful examination of their flame images suggests that the radius of curvature of the flame tip is close to $R = 0.24$ mm while the Markstein length for the $\phi = 0.88$ propane–air mixture examined is roughly $\mathcal{L} = 0.15$ mm [53]. Therefore, the ratio of the radius of curvature to the Markstein length below which differential-diffusion is found to play a role in [20] is $R/\mathcal{L} = 1.6$. To remain conservative, much larger radii of curvature of up to three times the Markstein length may be considered as potentially yielding differential-diffusion effects. In this study, using the methodology of [54], the Markstein lengths are evaluated to $\mathcal{L} = 0.209$ mm for propane flames at $\phi = 0.7$ and $\mathcal{L} = 0.146$ mm for methane flames at $\phi = 0.67$, leading to critical radii of curvature of $R = 0.627$ mm and $R = 0.438$ mm and critical curvatures of $\kappa = 1595$ m^{-1} and $\kappa = 2283$ m^{-1}, respectively. It is evident from Figs. 9(b) and (c) that such large magnitudes of curvature are not encountered with high probabilities in the flames examined here. Similar results are obtained for the other flames of this study (not shown here for conciseness). Therefore, differential-diffusion effects that are able to locally enhance or impair the burning velocity and heat release rate in the flames examined here are not statistically probable.

This can be confirmed by using the model developed by Preetham *et al*. [55], which suggests that the cutoff forcing frequency below which differential-diffusion plays no role in the dynamics of the present flames is $f = 1000$ Hz, which is much larger than the maximum forcing frequency considered here, $f = 400$ Hz. This model also shows that the hydrodynamic strain starts to play a role only for frequencies much higher than 1000 Hz. Therefore, differential-diffusion effects are ignored for the remaining analysis and the local burning velocity will be considered equal to the unstretched laminar burning velocity S_L.

C. Effects of the Laminar Burning Velocity

All the flames considered in this study reside in the “reaction sheet" regime of the Borghi diagram [56–59]. Therefore, the flames locally behave as laminar when interacting with turbulent eddies. In addition, from Figs. 5 and 6, the characteristic size of the AGV, obtained at phase $\theta = 188°$, can be estimated to be 6–10 mm, which is much larger than the flame thickness. For these reasons, the laminar burning velocity remains the controlling burning velocity on a microscopic level and it is expected to play a role on the FVR. As previously stated, the flame vortex roll-up mechanism is generated from the interaction of the toroidal vortex shed from the shear layer at the nozzle tip and the flame itself. The vortex propagates along the top region of the flame, modifying the flow field locally. At the same time, due to the modified flow field, the flame is pulled along with the vortex increasing its perimeter, and consequently, its surface area. The increase in flame surface area is then followed by a decrease that could be due to local quenching induced by the interaction with the vortex [60–64]. This fluctuation of the flame surface area results in the fluctuation of the global heat release from the flame. Higher values of laminar burning velocity could delay the local quenching [60] resulting in a greater increase of the surface area, and consequently, in a higher amplitude of global heat release fluctuation, *i.e.*,

higher FTF gain, during the forcing cycle. For this reason, the laminar burning velocity can be an important parameter controlling the FVR mechanism.

For all the conditions investigated, FVR_{max} is plotted in Fig. 11 as a function of S_L. The vertical error bars represent the uncertainty in the fitting process of the ellipse into the 0.4 iso-contour of normalized OH^* chemiluminescence intensity. The horizontal error bars represent the discrepancy in the value of S_L taken from the literature. The corresponding equivalence ratios are also reported in the graph.

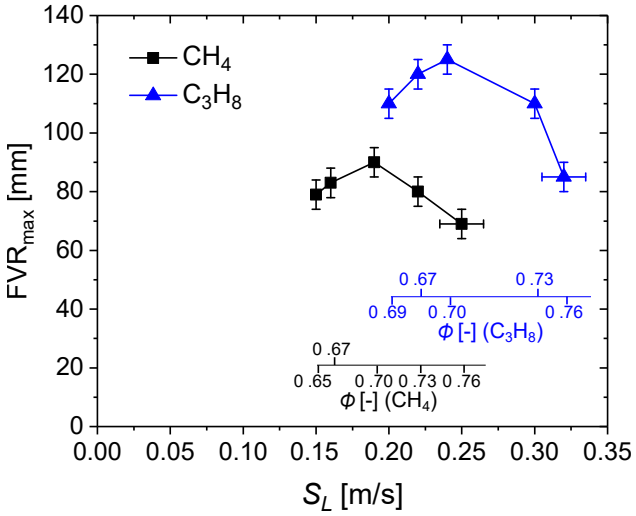

Fig. 11 The FVR_{max} at 176 Hz as a function of S_L for all the flames considered in this study.

For both fuels, FVR_{max} first increases with S_L and then decreases. For the three smallest equivalence ratios of each fuel, FVR_{max} is almost proportional to S_L. This can be explained by the fact that increasing the laminar burning velocity allows the flame to more readily conform to any change in the flow field, without being quenched, promoting flame vortex roll-up. However, the largest values of equivalence ratio for each fuel correspond to the lowest values of FVR_{max} even though S_L is large. This non-monotonic behavior suggests that other mechanisms are involved and that additional parameters play a role in controlling the maximum size of the FVR.

D. Effects of the Stabilization Distance on the AGV Circulation

As proposed by [62, 65], another parameter that needs to be considered in the FVR process is the circulation of the impinging acoustically generated vortex. According to [66], the circulation of a vortex, Γ, can be defined as the line integral over a closed contour, C, of the tangential component of the velocity, or as the integral over the cross-section area enclosed by C, A, of the vorticity component perpendicular to the cross-section area:

$$\Gamma = \oint_C \mathbf{u} \cdot \boldsymbol{ds} = \int_A \boldsymbol{\omega} \cdot \boldsymbol{dA} \tag{2}$$

Here, $\boldsymbol{ds}$ is a line element of the contour and $\boldsymbol{dA}$ is an element of the cross-section area. In this study, the circulation of the AGV is evaluated by integrating the vorticity over the cross-section area of the vortex delimited by the 0.5 iso-contour of the normalized Q-criterion. The temporal evolution of Γ over a forcing period is plotted in Fig. 12 for all the experimental conditions investigated. The error bar represents the uncertainty in the definition of the cross-section area of the vortex. The error bar is shown only for phase $\theta = 224°$ of the propane flame with $\phi = 0.69$. This is done in order to keep the graph readable. All the other data in the graph have similar uncertainties. From the planar velocity data, only the azimuthal vorticity can be determined. However, as the acoustic forcing is axisymmetric, the coherent structure that is generated is an azimuthal vortex that evolves in the measurement plane. Therefore, considering the circulation evaluated only from the azimuthal vorticity is a reasonable simplification.

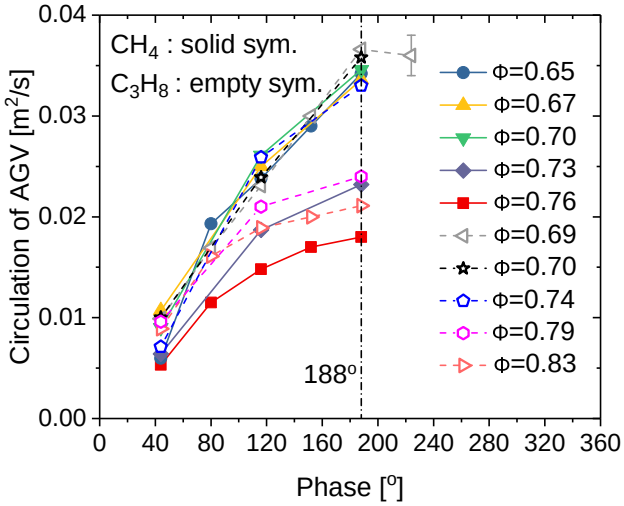

Fig. 12 Temporal evolution of the circulation of the AGV during the forcing cycle at 176 Hz for all the experimental conditions investigated in this study.

Regardless of fuel and equivalence ratio, the AGV circulation increases with time, after the AGV is being shed from the injector nozzle and while it is convected further downstream. The maximum value of the circulation, Γ_{max} is measured at phase $\theta = 188°$ for all the flames because for this value the AGV merges with the ORZ and its circulation cannot be determined anymore. Figure 12 shows that all the curves describing the temporal evolution of the AGV collapse within the experimental uncertainties, except for the two largest ϕ of each fuel. For both fuels, the two largest ϕ yield significantly smaller values of Γ_{max} over the whole forcing cycle. This suggests that the AGV is much weaker for the two largest ϕ of each fuel. This is corroborated by Figs. 5 and 6, where the largest ϕ exhibits the smallest AGV at $\theta = 188°$. It is important to note that the AGV circulation does not decrease continuously with ϕ. For each fuel, there exist a critical equivalence ratio below which the AGV circulation is not a function of ϕ. Above this threshold, the AGV circulation decreases suddenly and rapidly when ϕ is increased. The critical equivalence ratios are $\phi = 0.70$ and $\phi = 0.74$ for methane and propane, respectively. Additional values of equivalence ratio will be needed in order

to understand this sudden decrease in the value of the circulation with increasing the equivalence ratio. The sudden decrease in the value of FVR_{max} for the highest values of laminar burning velocity (see Fig. 11) could be due to the decrease in the maximum circulation of the AGV. When Γ_{max} decreases, the value of S_L is not high enough to keep increasing the FVR_{max}. This would result in an overall lower value of FVR_{max} for the largest laminar burning velocities.

It has been shown in previous studies [18, 19, 27, 67] that the interaction between the flame and the shear layers near the nozzle tip, where the AGV is shed, controls the properties of the AGV. In particular, Bunce *et al*. [18] suggested that the closer the flame is to the shear layer near the nozzle tip, the weaker is the AGV. This could be attributed to the increase of the temperature in the shear layer due to its closer proximity to the flame, which could affect gas expansion, baroclinic generation of vorticity, and viscous diffusion, and thereby reduce the circulation of the AGV [18, 62, 67–73].

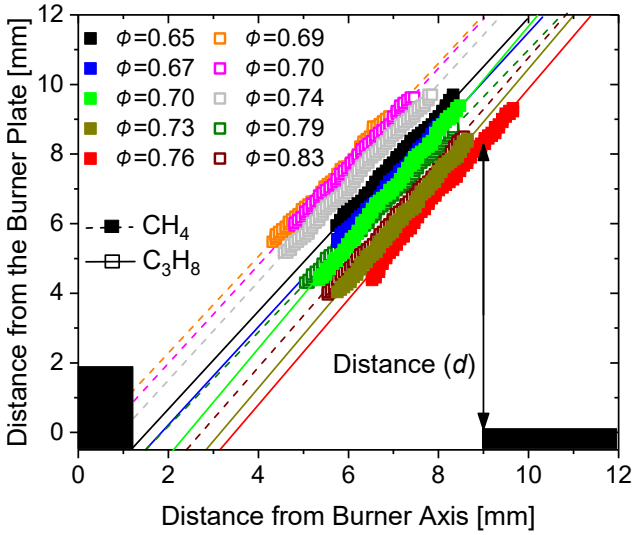

Fig. 13 Position of the flame front near the nozzle tip obtained from time averaged images of OH* chemiluminescence of unforced flames.

In order to verify if the distance from the flame to the shear layer may be responsible for the decrease of Γ_{max} observed for the largest ϕ, the position of the flame front near the nozzle tip is presented in Fig. 13. It is obtained from the time-averaged OH* chemiluminescence images of the unforced flames, without Abel deconvolution. After normalizing each image, a 0.4 iso-contour is considered. The square dots correspond to this iso-contour for each experimental condition. The dashed and solid lines are linear extrapolations of the flame fronts. Even though the value of the iso-contour (0.4) is somewhat arbitrary, choosing another value does not change the trend of the results. In the absence of acoustic forcing, the angle of the flame base is constant. It is not a function of fuel and equivalence ratio. More importantly, all the flames stabilize at different heights above the nozzle tip. For each fuel, flames featuring the largest ϕ are stabilized closer to the nozzle. In addition, for the same ϕ, methane flames sit closer to the nozzle than propane flames, even though their laminar burning velocities are smaller. The effect of fuel on the stabilization distance of premixed swirl flames will be the topic of further investigations.

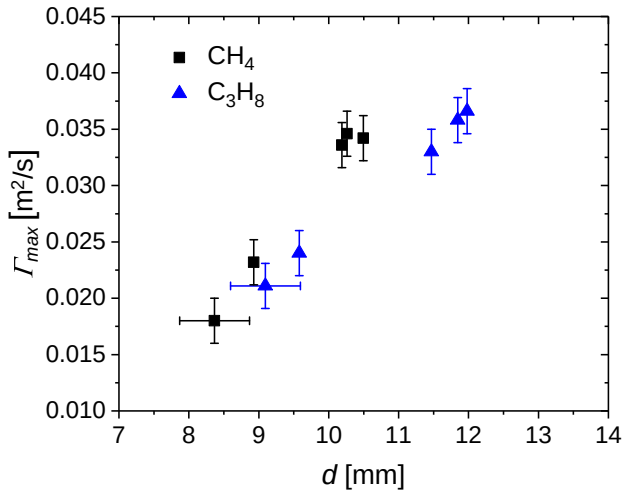

Fig. 14 The Γ_{max} as a function of d for all the cases examined in this study.

For each flame, it is possible to define a stabilization distance, d, as the length of a vertical line starting from the nozzle outer rim and ending as it intersects the linearly extrapolated flame front (colored lines in Fig. 13). The maximum circulation, Γ_{max}, is plotted as a function of the stabilization distance, d, in Fig. 14. For both fuels, Γ_{max} varies almost linearly with d. When the flame stabilizes close to the nozzle tip, the size of the AGV and its circulation are small. Note that there is a small difference between the two fuels. For a given stabilization distance, the strength of the AGV is consistently smaller for propane flames in comparison to methane flames. This could be explained by the fact that propane flames have a higher thermal power than methane flames for a similar bulk velocity (see Table 1), potentially resulting in a higher temperature in the shear layer near the nozzle tip.

E. Combined Effects of S_L and the AGV Circulation

In the previous subsections, it has been shown that increasing the equivalence ratio, and in turn the laminar burning velocity, has two competing effects on flame vortex roll-up. It promotes flame propagation but it also brings the flame closer to the nozzle, which weakens the AGV responsible for FVR. In this section, these combined and competing effects are discussed. In Fig. 15, the $\mathrm{FVR_{max}}$ is plotted as a function of the product of the laminar burning velocity and the maximum circulation of the AGV: $S_L \times \Gamma_{max}$. The $\mathrm{FVR_{max}}$ is almost proportional to this product. It could be argued that discrepancies lie within the rather large experimental uncertainties. Figure 15 confirms that both the laminar burning velocity and the circulation of the acoustically generated vortex are important parameters that control the flame vortex roll-up and, in turn, the dynamics of these premixed swirl flames at 176 Hz. These results also suggest that, for AGVs of equal circulation, the maximum size of the flame vortex roll-up as well as the FTF gain increases linearly with the laminar burning velocity. This is an important result that promotes the development of low-order models for the prediction of flame transfer functions. A corollary is that low-order models have no chance in predicting accurately

the FTF gain if they do not account for all the parameters controlling the generation and growth of the acoustically generated vortex during a forcing cycle.

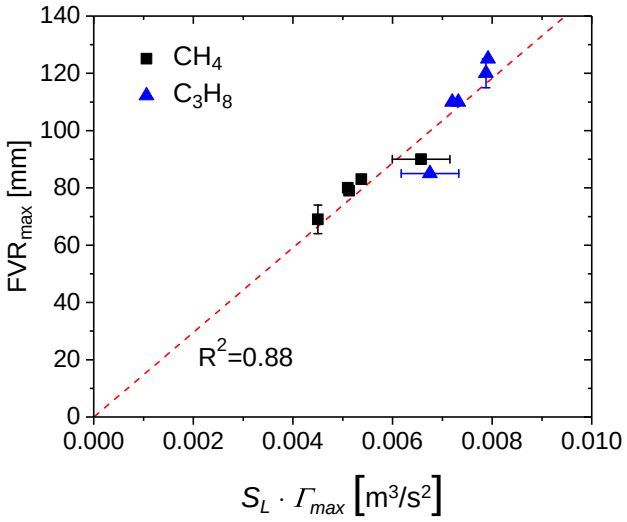

Fig. 15 The FVR_{max} at 176 Hz as a function of the product $S_L \times \Gamma_{max}$.

F. Effect of Flame Temperature on the AGV

In addition to the increase in S_L, an increase in ϕ induces an increase in flame temperature. This temperature increase could, in turn, increase the temperature in the shear layer and weaken the AGV. The laminar burning velocity as a function of the ratio of the adiabatic flame temperature, T_{ad}, over the temperature of the unburnt gases, T_u, is presented in Fig. 16. Since no temperature measurements are carried out, T_u is imposed equal to 300 K for all the experimental conditions. Figure 16 shows that S_L and T_{ad}/T_u are closely related and they might both weaken the AGV. On the other hand, the laminar burning velocity shows a broader range of variation (about a factor of 2) than T_{ad}/T_u (about 25%). From this, one can infer that the effect of the increase of the laminar burning velocity is perhaps dominant compared to the increase in flame temperature. Further study will be necessary to decouple these two effects and to investigate their relative importance.

G. Effect of Equivalence Ratio and Fuel on the FTF Phase

As shown earlier in the results section, the phase of the FTF at 176 Hz is also affected by the fuel and the equivalence ratio. For both fuels, increasing S_L decreases the stabilization distance, d, (see Fig. 13) as well as the distance between the tip of the flame and the nozzle (see Fig. 2). Since the bulk velocity $\bar{u}_{bulk}$ is similar in all the cases, the time lag between the oscillations of the velocity measured at the hot wire position and the fluctuations of the heat release rate, that mainly occur near the flame tip, is also reduced when S_L increases [5, 12, 25, 74]. This explains why the FTF phase consistently decreases with equivalence ratio for both fuels for forcing frequencies $f > 128$ Hz (see Fig. 3), where the

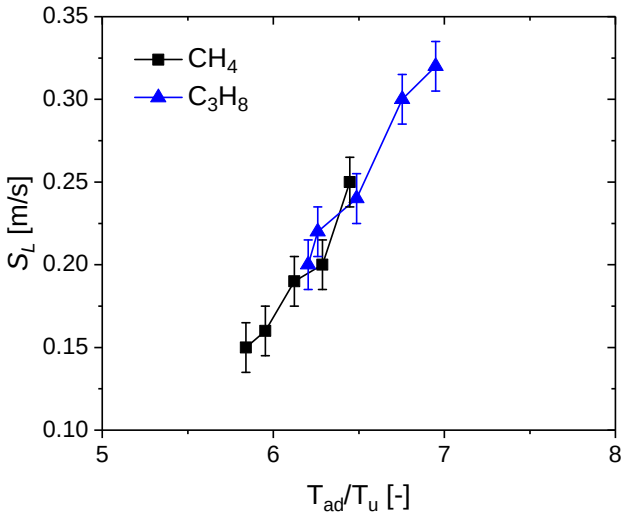

Fig. 16 Laminar burning velocity as a function of T_{ad}/T_u. The error bars represent the discrepancy in the values of S_L.

FVR controls the flame dynamics.

V. Conclusion

For both methane and propane lean premixed swirl flames, changing the equivalence ratio modifies the phase and the gain of the flame transfer functions in a similar fashion. The phase is affected only at frequencies higher than 112 Hz, which corresponds to the local minimum of the gain. The phase decreases when ϕ is increased. The gain is mainly a function of equivalence ratio at the forcing frequencies near 64 Hz, 176 Hz, and 336 Hz, that correspond to the three local maxima of the FTF gain. At 64 Hz and 176 Hz, a non-monotonic behavior of the FTF gain is observed as the equivalence ratio is increased. The magnitude of the FTF gain first increases with equivalence ratio but then decreases. At 336 Hz, the magnitude of the FTF gain increases monotonically with equivalence ratio. While focusing primarily on the forcing frequency corresponding to the second maximum of the FTF gain, 176 Hz, an analysis based on phase-locked images of OH^* chemiluminescence, OH-PLIF, and velocity fields is proposed.

The FTF gain and the maximum size of the flame vortex roll-up are proportional for all the flames considered. This is in agreement with a previous study conducted at elevated pressure, which underlines the fact that the flame vortex roll-up is an important mechanism controlling the response of these flames to acoustic forcing.

Based on the statistical analysis of the local curvature of the flame front, differential-diffusion effects have been ruled out and cannot explain the observed effects of fuel and equivalence ratio on the FTF gain and phase. The two main parameters controlling the flame vortex roll-up and the magnitude of the FTF gain at 176 Hz, are the laminar burning velocity S_L and the circulation of the vortex Γ. A proportionality relationship between the flame vortex roll-up maximum size and the product of S_L and Γ_{max} has been established. The laminar burning velocity influences the FTF

gain in two competing ways. Increasing the laminar burning velocity enhances the ability of the flame to conform to sudden flow changes and wrap around a vortex. On the other hand, increasing the laminar burning velocity reduces the distance between the flame base and the nozzle, which weakens the vortex generated by the acoustic forcing

For acoustically generated vortices of equal circulation, the maximum size of the flame vortex roll-up as well as the FTF gain increase linearly with the laminar burning velocity. This finding is useful for the development of low-order models dedicated to flame transfer function predictions. However, these experiments also show that low-order models cannot accurately predict the FTF gain unless all the parameters controlling the generation and growth of an acoustically generated vortex during a forcing cycle are taken into account.

Finally, to conclude on a more practical note, an empirical relationship between the magnitude of the FTF gain and the product $S_L \times \Gamma_{max}$ is proposed. This relationship could help engines designers to anticipate how different fuels or mixture compositions affect the response of the flame to acoustic perturbations. This could be a valuable tool for the development of new engines, since it could be used to assess these effects without carrying out expensive experiments or simulations.

Funding Sources

This work is funded by the King Abdullah University of Science and Technology, the Deutsche Forschungsgemeinschaft, and the Agence Nationale de la Recherche, through the GECCO project.

References

[1] Lefebvre, A., *Gas Turbine Combustion*, Taylor and Francis, Philadelphia, USA, 1998.

[2] Rayleigh, J. W. S., *The Theory of Sound*, Vol. 2, Macmillan, 1896. doi:10.1063/1.3060230.

[3] Candel, S., "Combustion Dynamics and Control: Progress and Challenges," *Proceedings of Combustion Institute*, Vol. 29, No. 1, 2002, pp. 1–28. doi:10.1016/S1540-7489(02)80007-4.

[4] Dowling, A. P., and Stow, S. R., "Acoustic Analysis of Gas Turbine Combustors," *Journal of Propulsion and Power*, Vol. 19, No. 5, 2003, pp. 751–764. doi:10.2514/2.6192.

[5] Lieuwen, T. C., and Yang, V., *Combustion Instabilities in Gas Turbine Engines*, Progress in Astronautics and Aeronautics, Vol. 210, AIAA, Reston, 2005. doi:10.2514/4.866807.

[6] Huang, Y., and Yang, V., "Dynamics and Stability of Lean-Premixed Swirl-Stabilized Combustion," *Progress in Energy and Combustion Science*, Vol. 35, No. 4, 2009, pp. 293–364. doi:10.1016/j.pecs.2009.01.002.

[7] Ducruix, S., Schuller, T., Durox, D., and Candel, S., "Combustion Dynamics and Instabilities: Elementary Coupling and Driving Mechanisms," *Journal of Propulsion and Power*, Vol. 19, No. 5, 2003, pp. 722–734. doi:10.2514/2.6182.

[8] Lieuwen, T. C., "Modeling Premixed Combustion–Acoustic Wave Interactions: A Review," *Journal of Propulsion and Power*, Vol. 19, No. 5, 2003, pp. 765–781. doi:10.2514/2.6193.

[9] Preetham, Santosh, H., and Lieuwen, T. C., "Dynamics of Laminar Premixed Flames Forced by Harmonic Velocity Disturbances," *Journal of Propulsion and Power*, Vol. 24, No. 6, 2008, pp. 1390–1402. doi:10.2514/1.35432.

[10] Noiray, N., Durox, D., Schuller, T., and Candel, S., "A Unified Framework for Nonlinear Combustion Instability Analysis Based on the Flame Describing Function," *Journal of Fluid Mechanics*, Vol. 615, 2008, pp. 139–167. doi:10.1017/S0022112008003613.

[11] Palies, P., Durox, D., Schuller, T., and Candel, S., "Nonlinear Combustion Instability Analysis Based on the Flame Describing Function Applied to Turbulent Premixed Swirling Flames," *Combustion and Flame*, Vol. 158, No. 10, 2011, pp. 1980–1991. doi:10.1016/j.combustflame.2011.02.012.

[12] Schuller, T., Durox, D., and Candel, S., "A Unified Model for the Prediction of Laminar Flame Transfer Functions: Comparisons between Conical and V-Flame Dynamics," *Combustion and Flame*, Vol. 134, No. 1-2, 2003, pp. 21–34. doi:10.1016/S0010-2180(03)00042-7.

[13] Bellows, B. D., Bobba, M. K., Forte, A., Seitzman, J. M., and Lieuwen, T. C., "Flame Transfer Function Saturation Mechanisms in a Swirl-Stabilized Combustor," *Proceedings of Combustion Institute*, Vol. 31, No. 2, 2007, pp. 3181–3188. doi:10.1016/j.proci.2006.07.138.

[14] Balachandran, R., Dowling, A. P., and Mastorakos, E., "Non-Linear Response of Turbulent Premixed Flames to Imposed Inlet Velocity Oscillations of Two Frequencies," *Flow, Turbulence and Combustion*, Vol. 80, No. 80, 2008, pp. 455–487. doi:10.1007/s10494-008-9139-1.

[15] Palies, P., Durox, D., Schuller, T., and Candel, S., "The Combined Dynamics of Swirler and Turbulent Premixed Swirling Flames," *Combustion and Flame*, Vol. 157, No. 9, 2010, pp. 1698–1717. doi:10.1016/j.combustflame.2010.02.011.

[16] Kim, K. T., Lee, J. G., Quay, B. D., and Santavicca, D. A., "Spatially Distributed Flame Transfer Functions for Predicting Combustion Dynamics in Lean Premixed Gas Turbine Combustors," *Combustion and Flame*, Vol. 157, No. 9, 2010, pp. 1718–1730. doi:10.1016/j.combustflame.2010.04.016.

[17] Kim, K. T., Lee, J. G., Quay, B. D., and Santavicca, D. A., "The Dynamic Response of Turbulent Dihedral V Flames: an Amplification Mechanism of Swirling Flames," *Combustion Science and Technology*, Vol. 183, No. 2, 2010, pp. 163–179. doi:10.1080/00102202.2010.508477.

[18] Bunce, N., Quay, B. D., and Santavicca, D. A., "Interaction between Swirl Number Fluctuations and Vortex Shedding in a Single-Nozzle Turbulent Swirling Fully-Premixed Flame Combustor," *Journal of Engineering for Gas Turbines and Power*, Vol. 136, No. 2, 2014, pp. 021503–1–11. doi:10.1115/1.4025361.

[19] Oberleithner, K., Schimek, S., and Paschereit, C. O., "Shear Flow Instabilities in Swirl-Stabilized Combustor and their Impact on the Amplitude Dependent Flame Response: A Linear Stability Analysis," *Combustion and Flame*, Vol. 162, No. 1, 2015, pp. 86–99. doi:10.1016/j.combustflame.2014.07.012.

[20] Gaudron, R., Gatti, M., Mirat, C., and Schuller, T., "Impact of the Injector Size on the Transfer Functions of Premixed Laminar Conical Flames," *Combustion and Flame*, Vol. 179, 2017, pp. 138–153. doi:10.1016/j.combustflame.2017.01.022.

[21] Külsheimer, C., and Büchner, H., "Combustion Dynamics of Turbulent Swirling Flames," *Combustion and Flame*, Vol. 131, No. 1-2, 2002, pp. 70–84. doi:10.1016/S0010-2180(02)00394-2.

[22] Kang, D., Culik, F., and Ratner, A., "Combustion Dynamics of a Low-Swirl Combustor," *Combustion and Flame*, Vol. 151, No. 3, 2007, pp. 412–425. doi:10.1016/j.combustflame.2007.07.017.

[23] Palies, P., Durox, D., Schuller, T., and Candel, S., "Experimental Study on the Effect of Swirler Geometry and Swirl Number on Flame Describing Functions," *Combustion Science and Technology*, Vol. 183, No. 7, 2011, pp. 704–717. doi:10.1080/00102202.2010.538103.

[24] Kim, K. T., Lee, J. G., Lee, H. J., Quay, B. D., and Santavicca, D. A., "Characterization of Forced Flame Response of Swirl-Stabilized Turbulent Lean-Premixed Flames in a Gas Turbine Combustor," *Journal of Engineering for Gas Turbines and Power*, Vol. 132, No. 3, 2010, pp. 041502–1–8. doi:10.1115/1.3204532.

[25] Durox, D., Schuller, T., and Candel, S., "Combustion Dynamics of Inverted Conical Flames," *Proceedings of Combustion Institute*, Vol. 30, No. 2, 2005, pp. 1717–1724. doi:10.1016/j.proci.2004.08.067.

[26] Durox, D., Schuller, T., Noiray, N., and Candel, S., "Experimental Analysis of Nonlinear Flame Transfer Functions for Different Flame Geometries," *Proceedings of Combustion Institute*, Vol. 32, No. 1, 2009, pp. 1391–1398. doi:10.1016/j.proci.2008.06.204.

[27] Palies, P., Schuller, T., Durox, D., Gicquel, L. Y. M., and Candel, S., "Acoustically Perturbed Turbulent Premixed Swirling Flames," *Physics of Fluids*, Vol. 23, No. 3, 2011, pp. 037101–1–15. doi:10.1063/1.3553276.

[28] Gatti, M., Gaudron, R., Mirat, C., Zimmer, L., and Schuller, T., "Impact of Swirl and Bluff-Body on the Transfer Tunction of Premixed Flames," *Proceedings of Combustion Institute*, Vol. 37, No. 4, 2019, pp. 5197–5204. doi:10.1016/j.proci.2018.06.148.

[29] Bellows, B. D., Neumeier, Y., and Lieuwen, T. C., "Forced Response of a Swirling, Premixed Flame to Flow Disturbances," *Journal of Propulsion and Power*, Vol. 22, No. 5, 2006, pp. 1075–1084. doi:10.2514/1.17426.

[30] Kim, K. T., and Hochgreb, S., "Effects of Nonuniform Reactant Stoichiometry on Thermoacoustic Instability in a Lean-Premixed Gas Turbine Combustor," *Combustion Science and Technology*, Vol. 184, No. 5, 2012, p. 608–628. doi:10.1080/00102202.2011.652788.

[31] Lacoste, D. A., Moeck, J. P., Durox, D., Laux, C. O., and Schuller, T., "Effect of Nanosecond Repetitively Pulsed Discharges on the Dynamics of a Swirl-Stabilized Lean Premixed Flame," *Journal of Engineering for Gas Turbines and Power*, Vol. 135, No. 10, 2013, pp. 101501–1–7. doi:10.1115/1.4024961.

[32] Di Sabatino, F., Guiberti, T. F., Boyette, W. R., Roberts, W. L., Moeck, J. P., and Lacoste, D. A., "Effect of Pressure on the Transfer Functions of Premixed Methane and Propane Swirl Flames," *Combustion and Flame*, Vol. 193, 2018, pp. 272–282. doi:10.1016/j.combustflame.2018.03.011.

[33] Di Sabatino, F., Lacoste, D. A., and Roberts, W. L., "A Detailed Characterization of a High Pressure Experimental Apparatus for Flame Dynamics Studies," *10th U.S. National Combustion Meeting*, April, 2017. Paper no. 2H03.

[34] Gupta, A. K., Lilley, D. G., and Syred, N., *Swirl Flows*, Abacus Press, Tunbridge Wells, England, 1984.

[35] Metghalchi, M., and Keckc, J. C., "Laminar Burning Velocity of Propane-Air Mixtures at High Temperature and Pressure," *Combustion and Flame*, Vol. 38, 1980, pp. 143–154. doi:10.1016/0010-2180(80)90046-2.

[36] Yamaoka, I., and Tsuji, H., "Determination of Burning Velocity using Counterflow Flames," *Symposium (International) on Combustion*, , No. 1, 1984, pp. 1883–1892. doi:10.1016/S0082-0784(85)80687-1.

[37] Yu, G., Law, C. K., and Wu, C. K., "Laminar Flame Speed of Hydrocarbon + Air Mixtures with Hydrogen Addition," *Combustion and Flame*, Vol. 63, No. 3, 1986, pp. 339–347. doi:10.1016/0010-2180(86)90003-9.

[38] Davis, S. G., and Law, C. K., "Determination of and Fuel Structure Effects on Laminar Flame Speeds of C_1 to C_8 Hydrocarbons," *Combustion Science and Technology*, Vol. 140, No. 1-6, 1998, pp. 427–449. doi:10.1080/00102209808915781.

[39] Zhao, Z., Kazakov, A., Li, J., and Dryer, F. L., "The Initial Temperature and N_2 Dilution Effect on the Laminar Flame Speed of Propane/Air," *Combustion Science and Technology*, Vol. 176, No. 10, 2004, pp. 1705–1723. doi:10.1080/00102200490487553.

[40] Mazas, A. N., Fiorina, B., Lacoste, D. A., and Schuller, T., "Effect of Water Vapor Addition on the Laminar Burning Velocity of Oxygen-Enriched Methane Flames," *Combustion and Flame*, Vol. 158, No. 10, 2011, pp. 2428–2440. doi: 10.1016/j.combustflame.2011.05.014.

[41] Goodwin, D., Moffat, H. K., and Speth, R. L., "Cantera: An Object-Oriented Software Toolkit for Chemical Kinetics, Thermodynamics, and Transport Processes," *Caltech, Pasadena, CA*, 2009.

[42] Wang, H., You, X., Joshi, A. V., Davis, S. G., Laskin, A., Egolfopoulos, F., and Law, C. K., "High-Temperature Combustion Reaction Model of H2/CO/C1-C4 Compounds," *USC Mech Version II*, 2007.

[43] Lee, J. G., and Santavicca, D. A., "Experimental Diagnostics for the Study of Combustion Instabilities in Lean Premixed Combustors," *Journal of Propulsion and Power*, Vol. 19, No. 5, 2003, pp. 735–747. doi:10.2514/2.6191.

[44] Balachandran, R., Ayoola, B. O., Kaminski, C. F., Dowling, A. P., and Mastorakos, E., "Experimental Investigation of the Nonlinear Response of Turbulent Premixed Flames to Imposed Inlet Velocity Oscillations," *Combustion and Flame*, Vol. 143, No. 1-2, 2005, pp. 37–55. doi:10.1016/j.combustflame.2005.04.009.

[45] Mercier, R., Guiberti, T. F., Chatelier, A., Durox, D., Gicquel, O., Darabiha, N., Schuller, T., and Fiorina, B., "Experimental and Numerical Investigation of the Influence of Thermal Boundary Conditions on Premixed Swirling Flame Stabilization," *Combustion and Flame*, Vol. 171, 2016, pp. 42–58. doi:10.1016/j.combustflame.2016.05.006.

[46] Jeong, J., and Hussain, F., "On the Identification of a Vortex," *Journal of Fluid Mechanics*, Vol. 285, 1995, pp. 69–94. doi:10.1017/S0022112095000462.

[47] Polifke, W., and Lawn, C., "On the Low-Frequency Limit of Flame Transfer Functions," *Combustion and Flame*, Vol. 151, No. 3, 2007, pp. 437–451. doi:10.1016/j.combustflame.2007.07.005.

[48] Komarek, T., and Polifke, W., "Impact of Swirl Fluctuations on the Response of a Perfectly Premixed Swirl Burner," *Journal of Engineering for Gas Turbines and Power*, Vol. 132, No. 6, 2010, pp. 061503–1–7. doi:10.1115/1.4000127.

[49] Jones, B., Lee, J. G., Quay, B. D., Santavicca, D. A., Kim, K., and Srinivasan, S., "Flame Response Mechanism due to Velocity Perturbations in a Lean Premixed Gas Turbine Combustor," *Journal of Engineering for Gas Turbines and Power*, Vol. 133, 2011, pp. 021503–1–9. doi:10.1115/1.4001996.

[50] Di Sabatino, F., Guiberti, T. F., Moeck, J. P., Roberts, W. L., and Lacoste, D. A., "Influence of the Laminar Burning Velocity on the Transfer Functions of Premixed Methane and Propane Swirl Flames," *Proceedings of ASME Turbo Expo.*, 2019. Not yet published.

[51] Palies, P., Durox, D., Schuller, T., and Candel, S., "Modeling of Premixed Swirling Flames Transfer Functions," *Proceeding of Combustion Institute*, Vol. 33, No. 2, 2011, pp. 2967–2974. doi:10.1016/j.proci.2010.06.059.

[52] Clavin, P., "Dynamic Behavior of Premixed Flame Fronts in Laminar and Turbulent Flows," *Progress in Energy and Combustion Science*, Vol. 11, No. 1, 1985, pp. 1–59. doi:10.1016/0360-1285(85)90012-7.

[53] Giannakopoulos, G. K., Gatzoulis, A., Frouzakis, C. E., Matalon, M., and Tomboulides, A. G., "Consistent Definitions of "Flame Displacement Speed" and "Markstein Length" for Premixed Flame Propagation," *Combustion and Flame*, Vol. 162, No. 4, 2015, pp. 1249–1264. doi:10.1016/j.combustflame.2014.10.015.

[54] Clavin, P., and Grana-Otero, J. C., "Curved and Stretched Flames: the Two Markstein Numbers," *Journal of Fluid Mechanics*, Vol. 686, 2011, pp. 187–217. doi:10.1017/jfm.2011.318.

[55] Preetham, Thumuluru, S. K., Santosh, H., and Lieuwen, T. C., "Linear Response of Laminar Premixed Flames to Flow Oscillations: Unsteady Stretch Effects," *Journal of Propulsion and Power*, Vol. 26, No. 3, 2010, pp. 524–532. doi:10.2514/1.41559.

[56] Law, C. K., *Combustion Physics*, Cambridge University Press, New York, USA, 2006. doi:10.1017/CBO9780511754517.

[57] Borghi, R., "On the Structure and Morphology of Turbulent Premixed Flame," *Recent Advances in the Aerospace Science*, 1985, pp. 117–138. doi:10.1007/978-1-4684-4298-4_7.

[58] Peters, N., "Laminar Flamelet Concepts in Turbulent Combustion," *Symposium (International) on Combustion*, Vol. 21, No. 1, 1986, pp. 1231–1250. doi:10.1016/S0082-0784(88)80355-2.

[59] Hawkes, E., Chatakonda, O., Kolla, H., Kerstein, A., and Chen, J., "A Petascale Direct Numerical Simulation Study of the Modeling of Flame Wrinkling for Large-Eddy Simulations in Intense Turbulence," *Combustion and Flame*, Vol. 159, No. 8, 2012, pp. 2690–2703. doi:10.1016/j.combustflame.2011.11.020.

[60] Poinsot, T., Veynante, D., and Candel, S., "Diagrams of Premixed Turbulent Combustion Based on Direct Simulation," *Symposium (International) on Combustion*, Vol. 23, No. 1, 1991, pp. 613–619. doi:10.1016/S0082-0784(06)80308-5.

[61] Roberts, W. L., and Driscoll, J. F., "A Laminar Vortex Interacting with a Premixed Flame: Measured Formation of Pockets of Reactants," *Combustion and Flame*, Vol. 87, No. 3, 1991, pp. 245–256. doi:10.1016/0010-2180(91)90111-N.

[62] Renard, P. H., Thevenin, D., Rolon, J. C., and Candel, S., "Dynamics of Flame/Vortex Interaction," *Progress in Energy and Combustion Science*, Vol. 26, No. 3, 2000, pp. 225–282. doi:10.1016/S0360-1285(00)00002-2.

[63] Echekki, T., and Kolera-Gokula, H., "A Regime Diagram for Premixed Flame Kernel-Vortex Interactions," *Physics of Fluids*, Vol. 19, 2007, p. 043604 (15). doi:10.1063/1.2720595.

[64] Thiesset, F., Halter, F., Bariki, C., Lapeyre, C., Chauveau, C., Gölkap, I., Selle, L., and Poinsot, T., "Isolating Strain and Curvature Effects in Premixed Flame/Vortex Interactions," *Journal of Fluid Mechanics*, Vol. 831, 2017, pp. 618–654. doi:10.1017/jfm.2017.641.

[65] Peters, N., and Williams, F. A., "Premixed Combustion in a Vortex," *Symposium (International) on Combustion*, Vol. 22, No. 1, 1988, pp. 495–503. doi:10.1016/S0082-0784(89)80056-6.

[66] Kundu, P. K., and Cohen, I. M., *Fluid Mechanics, Fourth Edition*, Academic Press, Burlington, USA, 2008.

[67] Kim, K. T., and Santavicca, D. A., "Interference Mechanisms of Acoustic/Convective Disturbances in a Swirl-Stabilized Lean-Premixed Combustor," *Combustion and Flame*, Vol. 160, No. 8, 2013, pp. 1441–1457. doi:10.1016/j.combustflame.2013.02.022.

[68] Soteriou, M. C., and Ghoniem, A. F., "The Vorticity Dynamics of an Exothermic, Spatially Developing, Forced, Reacting Shear Layer," *Symposium (International) on Combustion*, Vol. 22, No. 1, 1994, pp. 1265–1272. doi:10.1016/S0082-0784(06)80767-8.

[69] Coats, C., "Coherent Structures in Combustion," *Progress in Energy and Combustion Science*, Vol. 22, No. 5, 1994, pp. 427–509. doi:10.1016/S0360-1285(96)00011-1.

[70] Mueller, C. J., Driscoll, J. F., Reuss, D. L., Drake, M. C., and Rosalik, M. E., "Vortex Generation and Attenuation as Vortices Convect Through a Premixed Flame," *Combustion and Flame*, Vol. 112, No. 3, 1998, pp. 342–358. doi: 10.1016/S0010-2180(97)00122-3.

[71] Furi, M., Papas, P., Rais, M. R., and Monkewitz, P. A., "The Effect of Flame Position on the Kelvin-Helmholtz Instability in Non-Premixed Jet Flames," *Proceedings of Combustion Institute*, Vol. 29, No. 2, 2002, pp. 1653–1661. doi:10.1016/S1540-7489(02)80203-6.

[72] Shanbhogue, S., Plaks, D., and Lieuwen, T. C., "The K-H Instabilities of Reacting, Acoustically Excited Bluff Body Shear Layer," *Proceedings of 43rd AIAA Joint Propulsion Conference*, Cincinnati, OH, July 8-11, 2007, Paper no. 2007-5680. doi:10.2514/6.2007-5680.

[73] Emerson, B., O'Connor, J., Juniper, M., and Lieuwen, T. C., "Density Ratio Effects on the Reacting Bluff-Body Flow Field Characteristics," *Journal of Fluid Mechanics*, Vol. 706, 2012, pp. 219–250. doi:10.1017/jfm.2012.248.

[74] Kim, K. T., Lee, J. G., Quay, B. D., Santavicca, D. A., Kim, K., and Srinivasan, S., "Effect of Flame Structure on the Flame Transfer Function in a Premixed Gas Turbine Combustor," *Proceeding of ASME Turbo Expo*, 2008, paper no. GT2008-51014. doi:10.1115/1.3124664.